Pyridine Derivatives' Surface Passivation Enables Efficient and Stable Carbon-Based Perovskite Solar Cells

ACS MATERIALS LETTERS

www.acsmaterialsletters.org

LETTER

Pyridine Derivatives' Surface Passivation Enables Efficient and Stable Carbon-Based Perovskite Solar Cells

Kai Zou,[†] Qihua Li,[†] Jingquan Fan, Hebing Tang, Lixin Chen, Shuxia Tao,* Tingting Xu,* and Wei Huang

Cite This: *ACS Materials Lett.* 2022, 4, 1101−1111

Read Online

ACCESS | Metrics & More | Article Recommendations | Supporting Information

ABSTRACT: **Surface passivation has been demonstrated to be an effective strategy to reduce defects of hybrid halide perovskite films for making efficient and stable perovskite solar cells (PSCs). Especially the strong interaction between the passivation agents and the perovskite films is favorable for achieving a durable passivation effect. Pyridine derivatives with bidentate anchoring groups can interact with the uncoordinated Pb^{2+} and minimize perovskite defects. Herein, in order to rationally design bidentate passivation agents, the passivation effects of pyridine (Py) and its derivatives (Py-X) with different functional groups of amino, carboxyl acid, and aldehyde are compared in carbon-based perovskite solar cells (C-PSCs) for the first time. Py-NH_2 is found to passivate the perovskite $CH_3NH_3PbI_3$ film the best among all the passivation agents. The N atoms on both the pyridine ring and the amino group with lone pair electrons can combine with the uncoordinated Pb^{2+}, effectively reducing the defect density in the Py-NH_2-treated perovskite film. First-principles density functional theory (DFT) calculations reveal that the strong interaction between Py-NH_2 and $CH_3NH_3PbI_3$ strengthens Pb−I bond and hinders the formation of I vacancies. Carbon-based perovskite solar cells (C-PSCs) passivated by Py-NH_2 achieve a champion power conversion efficiency (PCE) of 14.75%, compared to 11.55% of the control device. The Py-NH_2 passivated C-PSCs also exhibit good long-term stability, retaining more than 90% of the initial efficiency after 30 days of storage in air with 35−45% relative humidity.**

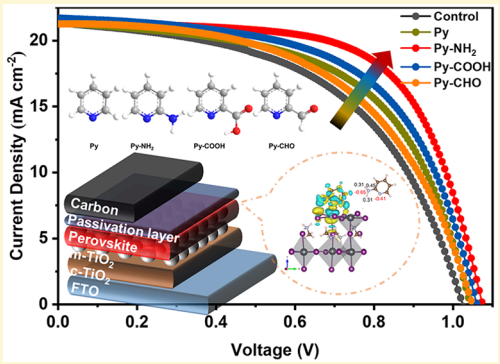

Organic−inorganic hybrid perovskite materials general refer to a class of materials with the crystal structure ABX_3, where A is an organic cation of methylamine (MA) or formamidine (FA), B is Pb or a tin-based metal, and X is a halide ion. Perovskite materials are widely used in optoelectronic devices due to their high absorption coefficient, large carrier mobility, long diffusion length, and easy solution processing properties.[1,2] As an emerging rising star material in the photovoltaic area, metal halide perovskite solar cells (PSCs) have gained rapid progress, with power conversion efficiency (PCE) increasing from the initial 3.9% in 2009 to 25.7% at present.[3,4] The PCE growth of PSCs has a much faster rate than that of dye-sensitized solar cells.[5,6] Besides the factors of charge-transporting layers, interfacial layers, and device architecture, the high photovoltaic performance of PSCs mainly relies on uniform coating of the light absorbing perovskite with an appropriate crystal grain size and few defects. Defects may form as the nonradiative recombination centers consume free carriers, and they can also trigger perovskite film decomposition, thus affecting the open circuit voltage (V_{oc}), fill factor (FF) and long-term stability of PSCs.[7] Structural defects of perovskite materials include (1) intrinsic defects, also known as point defects, such as vacancy, interstitial and Pb−I antisite replacement, and (2) impurity-based defects originated by doped ions etc.[8] With the expected above-mentioned structural defects, solution-processed perovskite films may generate a large number of defects on the surface or at the grain boundaries during the film preparation process. In $MAPbI_3$-based perovskite materials, the organic MA group is easily released from the perovskite crystal lattices during the thermal annealing process to create organic cation vacancies.[9] The halide anion vacancies are formed due to the undercoordinated Pb^{2+} defects. Reports

Received: February 9, 2022
Accepted: April 28, 2022
Published: May 6, 2022

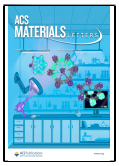

https://doi.org/10.1021/acsmaterialslett.2c00123
ACS Materials Lett. 2022, 4, 1101−1111

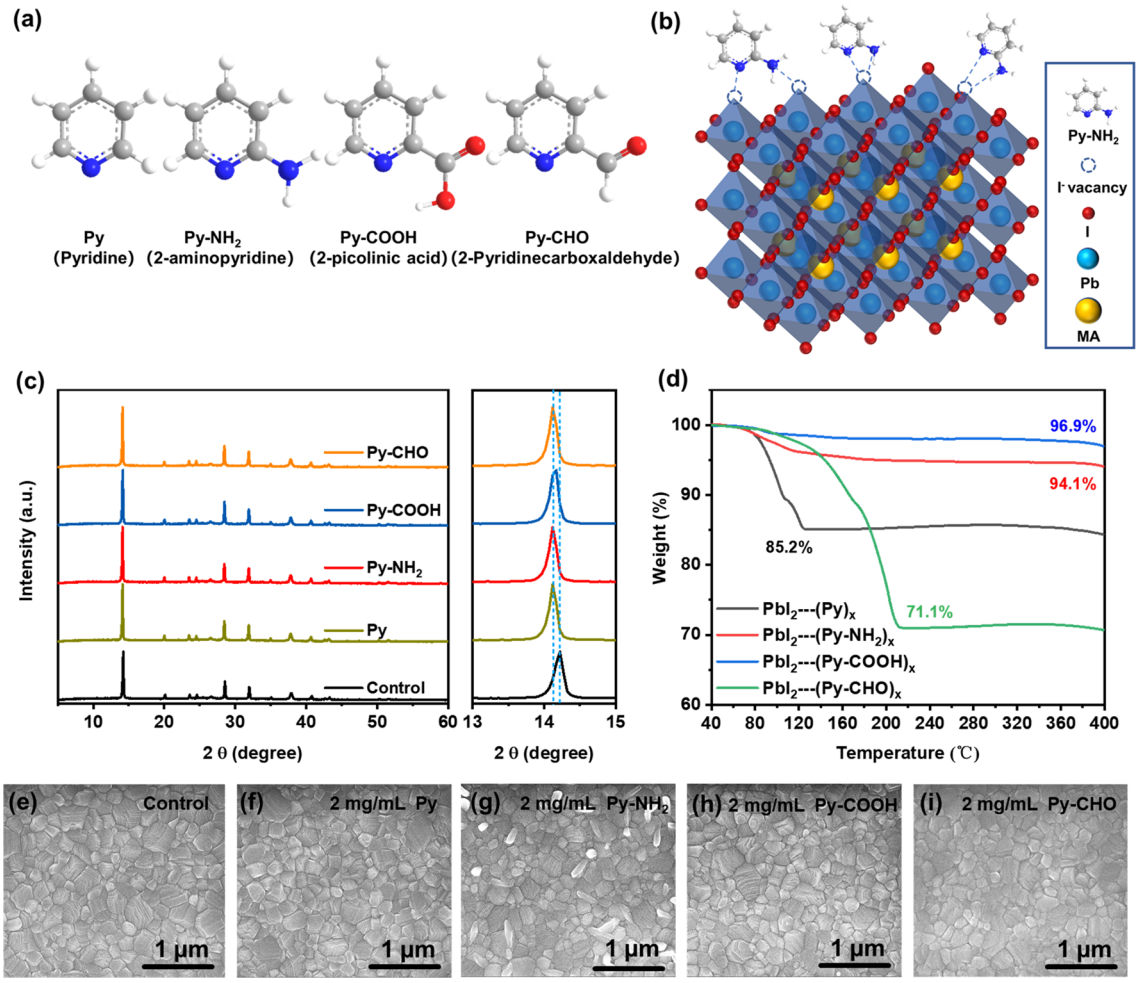

Figure 1. (a) Chemical structures of the passivation molecules used in the study: pyridine (Py), 2-aminopyridine (Py-NH_2), 2-carboxypyridine (Py-COOH), and 2-aldehydepyridine (Py-CHO); (b) schematic diagram of Py-NH_2 molecules interacted with perovskite; (c) XRD patterns of perovskite films with and without Py-X treatment; (d) thermogravimetric curves of PbI_2-(Py-X)$_x$ complex powders; (e–i) field emission scanning electron microscopy images of perovskite films passivated with and without Py-X.

showed that the undercoordinated ions at the crystal surface may accumulate excess positive carriers at the heterojunction of the perovskite/HTM interface.[10] Therefore, minimizing defects in the perovskite materials and PSCs is obviously an important direction to boost photovoltaic performance and long-term stability.

Surface passivation effectively reduces defects and suppresses ion movement on the surface or at the grain boundaries of perovskite films.[11−14] Many small molecules and polymers were used as surface passivation agents to reduce defects on the surface and grain boundaries of perovskite films.[15−20] The uncoordinated Pb^{2+} can be passivated by Lewis bases having electron donating atoms (N, O, or S, etc.) via coordination bonding, eliminating positively charged defects. Passivation molecules with an amino or carboxyl functional group can react with the Pb^{2+} to form ionic bonding through an electrostatic interaction.[16,21] In order to achieve robust passivation, the binding strength between passivation molecules and perovskite films is crucial for reliable passivation. Passivation agents having multiple ligands or functional groups can increase the stability of the metal−ligand complex because of the enhanced chelate effect or having more reaction sites. Zhu et al. demonstrated the bidentate molecule of 2-mercaptopyridine (2-MP) increased anchoring strength and obtained enhanced PCE and stability.[22] Yang et al. found that passivation with strong interaction energy promotes effective defect passivation, and inhibits defect migration as well.[23] A surface passivation agent not only can passivate surface defects of perovskite, it can also be applied as an interfacial modifier to reduce energy level mismatching between perovskite and the carbon electrode.[24,25] Our group previously reported a 2-amino-5-(trifluoromethyl)pyridine (5-TFMAP) passivation agent with bidentate groups to passivate the perovskite $CH_3NH_3PbI_3$ films.[26] The two anchoring sites of a NH_2 group and a pyridine ring provided strong interaction with the undercoordinated Pb^{2+}, efficiently reducing the defect states of perovskite films, promoting better carrier transport and inhibiting nonradiative recombination.

In this work, we purposely choose several pyridine derivatives as passivation agents, namely pyridine (Py), 2-aminopyridine with an amino group (Py-NH_2), 2-picolinic acid with a carboxyl group (Py-COOH), and 2-pyridinecarboxaldehyde with an aldehyde group (Py-CHO). The aim of this study is to reveal the functional groups' effects in the bidentate passivation agents. A synergy effect of functional groups would be a challenge for designing good passivation agents for perovskite. Herein, the molecular interactions of pyridine and its derivatives with perovskite films were extensively investigated by Fourier transform infrared spectroscopy (FTIR), nuclear magnetic

https://doi.org/10.1021/acsmaterialslett.2c00123
ACS Materials Lett. 2022, 4, 1101−1111

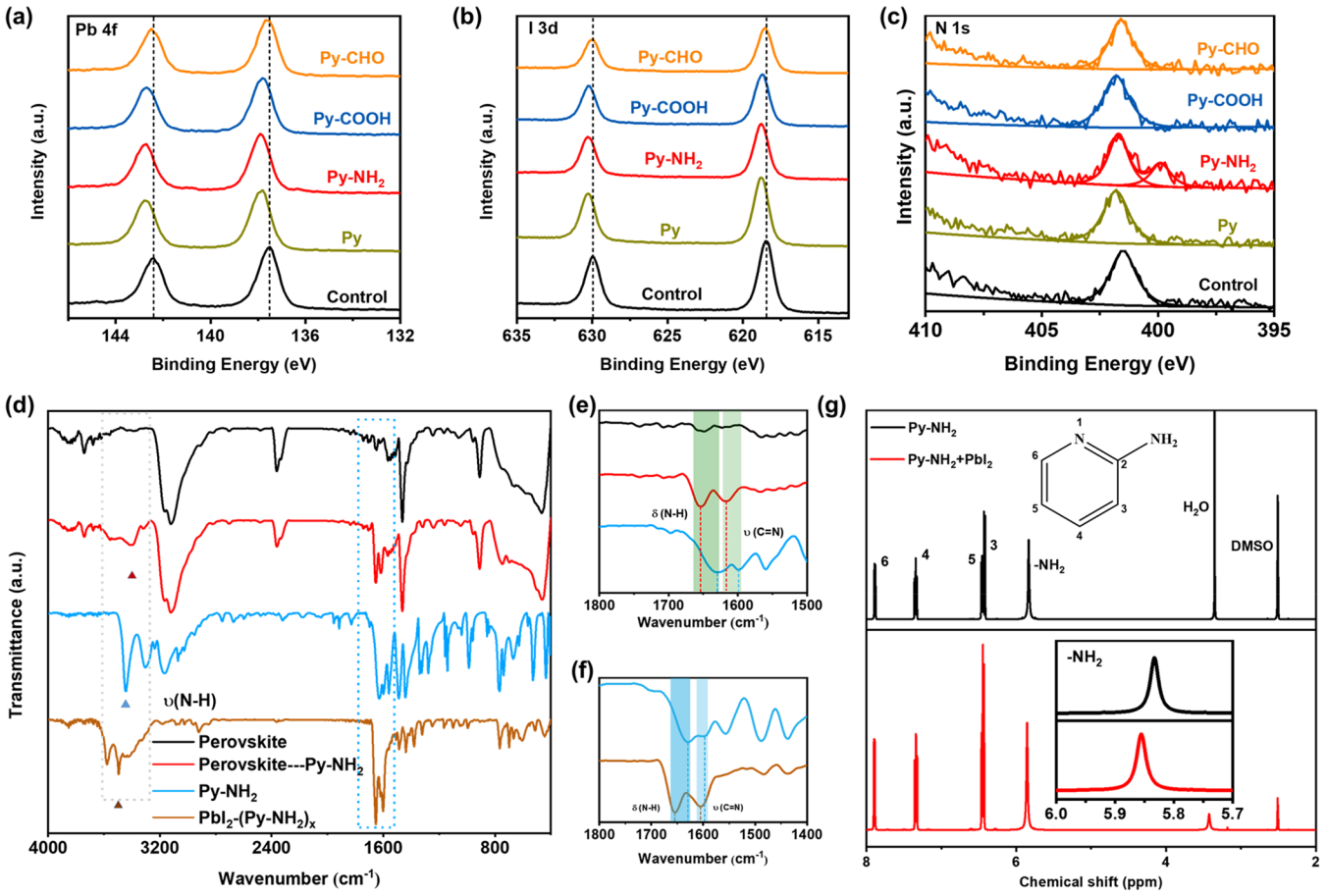

Figure 2. X-ray photoelectron spectroscopy (XPS) of perovskite films with and without Py-X passivation treatment: (a) Pb 4f core-level spectra; (b) I 3d core-level spectra; (c) N 1s core-level spectra; (d, e, f) FTIR spectra of Py-NH_2, the Py-NH_2 complex with PbI_2, pristine perovskite, and Py-NH_2-treated perovskite; (g) proton nuclear magnetic resonance (^{1}H NMR) spectroscopy of Py-NH_2 and its mixed solution with PbI_2 (dissolved in DMSO-d6 solvent).

resonance (NMR) spectroscopy, and X-ray spectroscopy (XPS), etc. 2-Aminopyridine (Py-NH_2) gives the best passivation effect in terms of the photovoltaic performance of carbon-based perovskite solar cells (C-PSCs). Py-NH_2 passivated perovskite films presented superior quality of improved carrier lifetime and carrier transport properties. First-principles density functional theory (DFT) calculations confirm the strong interaction between Py-NH_2 and $CH_3NH_3PbI_3$, strengthening the Pb−I bond and impeding the formation of I vacancies. The power conversion efficiency of the C-PSCs passivated by Py-NH_2 is 14.75%, while that of the control device is only 11.55%. For long-term stability, Py-NH_2 passivated PSCs retained more than 90% of the initial efficiency after 30 days of storage in air with 35−45% relative humidity. This work might provide good insight for appropriately designing efficient and reliable bidentate passivation molecules for the perovskite field.

Figure 1a shows the molecular structures of passivation agents of pyridine and its derivatives (Py-X). Four representative functional groups on the pyridine ring were purposely chosen to evaluate the passivation effects on the perovskite $CH_3NH_3PbI_3$ surface. Bidentate anchoring groups of pyridine derivatives would provide stronger strength than that of the sole reaction site of pyridine. Figure 1b shows a proposed mechanism of Py-NH_2-treated perovskite film defects. As a Lewis base, the N atom on the pyridine ring and the N atom on the amino group can interact with undercoordinated Pb^{2+}; thus, I vacancy defects on the surface or grain boundaries of perovskite films can be reduced. Passivation treatment could lead to good cell performance and long-term stability of devices.

The X-ray diffraction (XRD) spectrum in Figure 1c shows the control and the surface passivated perovskite films. The films all showed characteristic perovskite diffraction peaks of the (110) plane around 14°. No characteristic peak of PbI_2 was observed after passivation. From the amplified spectrum at the (110) plane (right figure), the peaks of the passivated perovskite films all move to a lower degree (about 0.1°) compared to the control film. Due to the absorption and desorption of the pyridine derivatives on the perovskite surface, the perovskite lattice was affected by the pyridine and its derivatives. Interestingly, in our previous study, there is no XRD peak shift when the larger pyridine derivative 2-amino-5-(trifluoromethyl)pyridine (5-TFMAP) was used to treat the perovskite film.[26] This may be due to the steric size effect of 5-TFMAP. For crystallinity comparison, the full width at half-maximum (fwhm) values of these films were calculated; the Py-NH_2-treated film has the lowest fwhm value of 0.112 among all the other films, with the comparison to the value of 0.136 for the control film. The results indicate that the crystallinity and grain size of perovskite films are improved after Py-NH_2 treatment.

The phase stability and thermal properties of the PbI_2-(Py-X)$_X$ complex (preparation method in the Supporting Information, photographs of the solution mixture and the solid complex shown in Figure S1) were investigated by

https://doi.org/10.1021/acsmaterialslett.2c00123
ACS Materials Lett. 2022, 4, 1101−1111

thermogravimetric analysis (TGA). Figure 1d shows TGA profiles of various PbI_2-(Py-X)$_X$ complexes. PbI_2-(Py-NH_2)$_X$ and PbI_2-(Py-COOH)$_X$ showed excellent thermal stability with less than 10% weight loss after being heated to 400 °C, while PbI_2-(Py)$_X$ and PbI_2-(Py-CHO)$_X$ had dramatic weight loss after being heating to 120 and 210 °C, respectively. The final weight percentage after heating at 400 °C is 85.2% and 71.1% for PbI_2-(Py)$_X$ and PbI_2-(Py-CHO)$_X$, respectively. The reason for this might be that the binding force of Py-NH_2 or Py-COOH with PbI_2 is much stronger while the interaction of Py or Py-CHO with PbI_2 is relatively weaker, thus they may be decomposed at their respective boiling points. The TGA results suggest that binding of Py-NH_2 and Py-COOH with PbI_2 is thermally more stable than that of the other two complexes.[17,22]

In order to further verify the interaction between Py-X and PbI_2, the XRD spectra of PbI_2-(Py-X)$_X$ powder rather than the perovskites were measured as shown in Figure S2. The characteristic diffraction peak of PbI_2 at the (001) plane for both PbI_2-(Py-NH_2)$_X$ and PbI_2-(Py-COOH)$_X$ complexes disappeared in Figure S2a and b, confirming complete formation of complex due to the strong interaction between PbI_2 and Py-NH_2 and Py-COOH, respectively. For the PbI_2-(Py)$_X$ and PbI_2-(Py-CHO)$_X$ complexes, the characteristic peak of PbI_2 can still be observed with much reduced peak intensity, indicating the PbI_2 might remain due to the weak interaction of Py and Py-CHO with PbI_2, respectively. The above XRD results of the PbI_2-(Py-X)$_X$ complex show that the interaction between Py-X and PbI_2 may strongly depend on the side group in the pyridine ring.

The morphology of perovskite films was examined by field emission scanning electron microscopy (FESEM) as shown in Figure 1e−i. The pristine and passivated perovskite films all showed uniform coverage on substrates. The average grain size of the films is shown in Figure S3. Compared with the original perovskite film having a grain size of 178 (±42) nm, the grain size of the perovskite films after passivation followed the order Py-NH_2 (203 ± 32 nm) > Py-COOH (191 ± 38 nm) > Py (188 ± 36 nm) > Py-CHO (156 ± 30 nm). Py-NH_2-treated perovskite films presented a small amount of white stripes on film surface as shown in Figure 1f. Except Py-NH_2, the other Py-X-treated perovskite films had almost similar morphology as the control film. The solvent effect from chlorobenzene (CB) was also excluded as provided from the SEM and XRD results in Figure S4 of the Supporting Information. A high concentration (10 mg/mL) of passivation agents was applied to check the morphology changes in Figure S5. A large amount of Py-NH_2 and Py-COOH can dramatically change the film morphology, leading to strip shaped and porous surfaces, respectively.

The surface roughnesses of the pristine and passivated perovskite films were tested by atomic force microscopy (AFM) as shown in Figure S6. The roughness of the Py-NH_2-treated perovskite film showed the lowest root-mean-square roughness (RMS) of 9.24 nm among all the films. The smooth perovskite film is good for closely contacting with the carbon electrode.

In order to further study the interaction between pyridine derivatives and perovskite films, perovskite films before and after passivation were tested by X-ray photoelectron spectroscopy (XPS) as shown in Figure 2a and c. Full XPS survey spectra of perovskite films are shown in Figure S7a. High-resolution XPS spectrum of Pb 4f in Figure 2a shows that the binding energies of the two main peaks of Pb $4f_{7/2}$ and Pb $4f_{5/2}$ for the original perovskite films are 137.5 and 142.4 eV, respectively. Surface passivation treatment leads to the peaks shifting to a higher energy direction; that is, the binding energies of the Pb $4f_{7/2}$ and Pb $4f_{5/2}$ peaks for the Py, Py-NH_2, and Py-COOH passivated perovskite films were all shifted to the higher value 137.9 and 142.8 eV, which is 0.4 eV higher than those of the original film. While for the Py-CHO-treated film, the binding energies of the two peaks were shifted to 137.6 and 142.5 eV, 0.1 eV higher than those of the untreated film. The corresponding binding energy of Pb 4f shifts toward higher binding energy after passivation, which confirmed the interaction between the passivation agents and Pb^{2+}. Compared with Py-CHO, we found that the shifts of Py, Py-NH_2, and Py-COOH were larger, indicating that Py, Py-NH_2, and Py-COOH interact with Pb^{2+} more strongly. This is consistent with the results observed by Yang et al.[23] Moreover, this shift may also be related to changes of the Pb−I bond length.[27] The high-resolution XPS spectrum of I 3d in Figure 2b also shows a similar phenomenon as that of the Pb 4f spectrum. After Py, Py-NH_2, and Py-COOH treatment, a bigger movement for the main peaks of I $3d_{5/2}$ and I $3d_{3/2}$ occurs than that of the Py-CHO passivated films.

As shown in the N 1s high-resolution spectrum of Figure 2c, the N 1s peak of the original film was located at 401.5 eV, and it moved toward the higher binding energy side after treatment with Py, Py-NH_2, and Py-COOH agents. The Py-CHO-treated film had less movement compared with the other three passivated films. This may be due to weak interaction between Py-CHO and perovskite films. For the Py-NH_2 passivated film, a peak associated with the amino group was observed at 399.9 eV, indicating that Py-NH_2 might exist on the surface of the perovskite film. The main peak of O 1s provided in Figure S7b of the Supporting Information. A peak at 532.4 eV for all the films might be attributed to O_2 and H_2O in air.[28] An additional peak at 533.6 eV for Py-CHO-treated perovskite films corresponded to the aldehyde group on Py-CHO, indicating the existence of the Py-CHO molecule on the surface of the perovskite film.[29]

Fourier transform infrared spectroscopy (FTIR) is a powerful tool to identify functional group changes. In order to elucidate interaction between passivation agents and perovskite, FTIR spectra of the Py-NH_2 agent, the complex PbI_2−Py-NH_2, and perovskite films before and after Py-NH_2 passivation were recorded as shown in Figure 2d and f. Compared with Py-NH_2 itself, the Py-NH_2 passivated perovskite film (red line) and PbI_2-(Py-NH_2)$_x$ complex (brown line) showed that the bending vibration peak of the N−H bond in the amino group shifted from 1629.5 to 1653.9 cm^{-1} and 1654.7 cm^{-1}, respectively. The stretching vibration peak of the N−H bond moved from 3445.1 to 3400.4 cm^{-1} and 3493.8 cm^{-1}, respectively. The stretching vibration peak of the C═N bond in the pyridine ring also shifted from 1597.4 to 1616.7 cm^{-1} for the Py-NH_2 passivated perovskite film (Figure 2e) and to 1605.4 cm^{-1} for the PbI_2-(Py-NH_2)$_x$ complex (Figure 2f). This suggested that Py-NH_2 acts as a bidentate ligand to passivate defects by interacting with uncoordinated Pb^{2+} in perovskite films. Figure S8 shows the FTIR spectra of Py-, Py-COOH-, and Py-CHO-treated perovskite films. Py-treated PbI_2 and perovskite film showed peak shifts for the stretching vibration of C═N in the pyridine ring in Figure S8a. In the FTIR spectra of the PbI_2-(Py-COOH)$_x$ complex and surface-treated perovskite films (Figure S8d), the stretching vibration peak of the C═O bond in the -COOH group and the stretching vibration peak of C═N in the pyridine ring both shifted accordingly, indicating Py-COOH has strong interaction with uncoordinated Pb^{2+} in perovskite films. For Py-CHO-treated perovskite films as shown in Figure S8g, there is

https://doi.org/10.1021/acsmaterialslett.2c00123
ACS Materials Lett. 2022, 4, 1101−1111

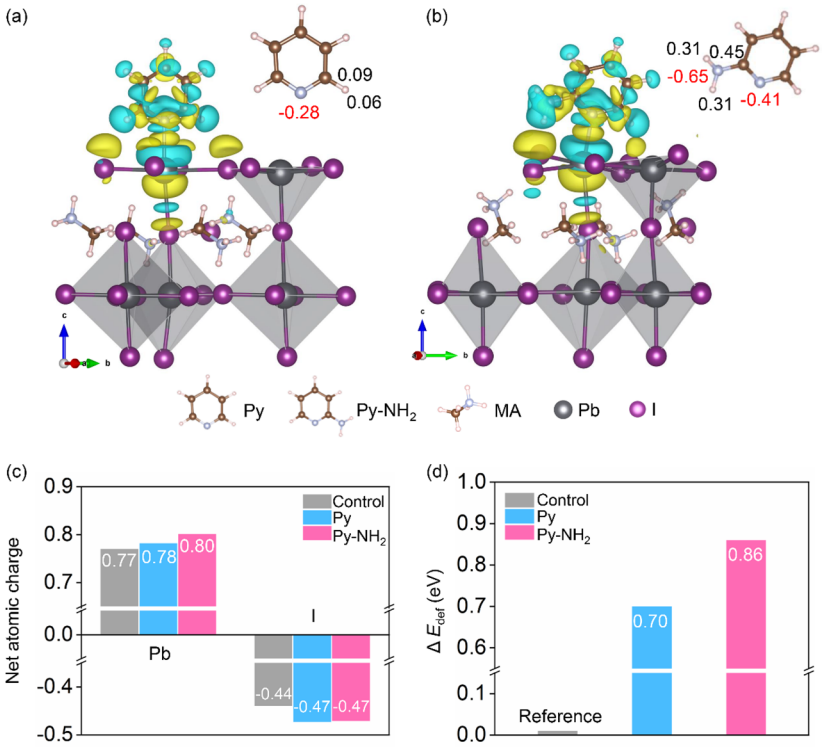

Figure 3. Theoretical analysis of the interaction between Py (a)/Py-NH_2 (b) and $MAPbI_3$. Both parts a and b contain information on the most stable configuration of the Py- or Py-NH_2@PbI_2-terminated surface, the net atomic charge of Py or Py-NH_2 (the value of the N_{ring} is highlighted in red, while the adjacent atoms are in black), and the charge transfer between Py and $MAPbI_3$, for which yellow represents the accumulation of charge and cyan represents the depletion of charge. The net atomic charge of Pb interacts with Py and Py-NH_2 and the I atom beneath the Pb in the reference (clean PbI_2-terminated surface) and Py- and Py-NH_2@PbI_2-terminated surfaces (c). Formation energy differences of the I vacancy (I54) in the Py- and Py-NH_2@PbI_2-terminated surfaces compared to the control (clean PbI_2-terminated) surface (d).

no corresponding peak change, and this may be due to the escape of Py-CHO during the annealing process. This further indicates that the binding ability of Py-CHO on the perovskite film surface is poor. In the FTIR spectra of the PbI_2-$(Py\text{-}CHO)_x$ complex in Figure S8g, no change in the stretching vibration peak of the C═N bond related to the pyridine group was observed either, again confirming the weak interaction between Py-CHO and PbI_2.

In order to further verify the chemical interaction between Py-X and Pb^{2+}, the ^{1}H NMR spectra of the Py-NH_2 molecule and PbI_2-$(Py\text{-}NH_2)_x$ complex were measured in DMSO-*d6*, as shown in Figure 2g. The chemical shift of the H in the -NH_2 group moved to a lower field (from 5.83 to 5.86 ppm), and this may be due to the formation of a coordination bond between -NH_2 and Pb^{2+}. The ^{1}H NMR spectra of other passivation agents were also studied as shown in the Figure S9 of the Supporting Information. No noticeable changes for Py and Py/PbI_2 can be observed, since the H atom is far away from the interaction site in the pyridine ring. Py-COOH has a broad peak centered at 3.43 ppm in the ^{1}H NMR spectrum of Figure S9b. However, this peak disappeared in the spectrum of Py-COOH/PbI_2, suggesting that there is interaction between the passivation agent and PbI_2. The chemical shift of H in the Py-CHO-PbI_2 complex slightly shifted from 9.99 to 9.98 ppm to the higher field, showing that the -CHO group in Py-CHO also has the ability to form a coordination bond with Pb^{2+}, but the interaction force is relatively weak, which is consistent with the FTIR results.

In order to provide insight into the passivation effects of Py and Py-NH_2 on $MAPbI_3$, we further studied the atomistic interactions between Py/Py-NH_2 and $MAPbI_3$ by using DFT calculations. We started with their adsorption on $MAPbI_3$, and their adsorption strength is characterized by the adsorption energy (E_{ads}), which was calculated following the equation $E_{ads} = E_{molecule@MAPbI3} - E_{MAPbI3} - E_{molecule}$ ($E_{molecule@MAPbI3}$, E_{MAPbI3}, and $E_{molecule}$ are the total energies of Py/Py-NH_2 adsorption on the surface of $MAPbI_3$, the $MAPbI_3$ surface, and Py/Py-NH_2, respectively). Several possible adsorption sites of Py and Py-NH_2 on both the PbI_2- and MAI-terminated perovskite surfaces were considered in Figure S10. The adsorption energies fall in the range from −0.04 to −0.75 eV for the Py-NH_2@$MAPbI_3$ system and from −0.07 to −1.12 eV for the Py@$MAPbI_3$ system in Table S1, indicating strong interactions of both Py and Py-NH_2 with the $MAPbI_3$ surface. We note that the PbI_2-terminated surface is preferential over the MAI-terminated one for both Py and Py-NH_2, with the most negative E_{ads} of −1.12 eV for Py and −0.75 eV for Py-NH_2. This indicates both molecules can strongly interact with dangling Pb species. Interestingly, as shown in Figure S10, because of the availability of two electronegative N species in Py-NH_2, it can bind strongly with the Pb in several possible configurations.

To understand the consequence of the strong interaction between Py and Py-NH_2 with Pb, we zoom into the most stable configurations in Figure 3a and b, where we find strong interaction of the N atom from the rings of Py and Py-NH_2 with Pb, evidenced by the electron transfer from Pb to the N_{ring} of Py/Py-NH_2. This can be attributed to the strong electron attraction ability of the N_{ring} of Py/Py-NH_2, which can be seen from the net atomic charge (NAC) of the N_{ring} of Py (−0.28) and Py-NH_2 (−0.41). The strong N−Pb interactions seen in our calculations

https://doi.org/10.1021/acsmaterialslett.2c00123
ACS Materials Lett. 2022, 4, 1101−1111

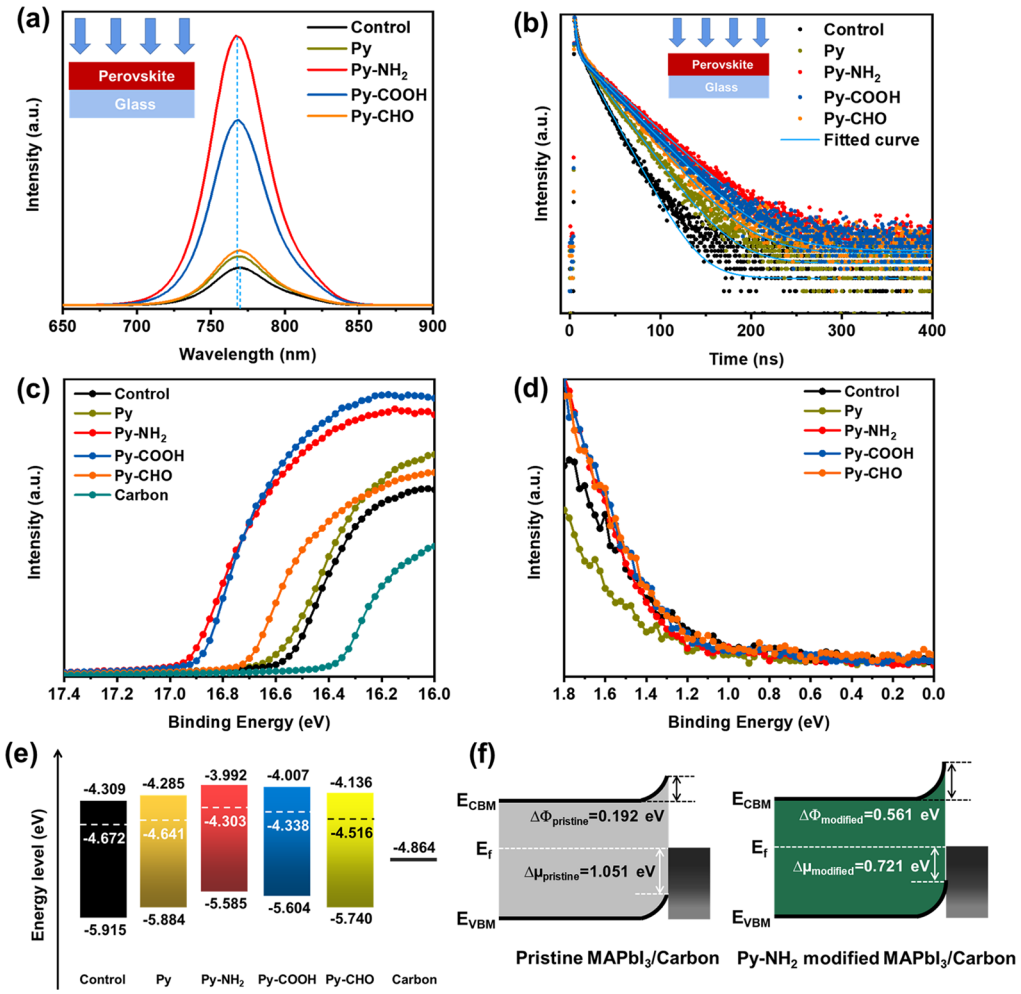

Figure 4. Steady-state fluorescence (PL) and time-resolved photoluminescence (TRPL) decay spectra of perovskite film on glass substrates (a and b). The films were excited by a laser at 510 nm. Ultraviolet photoelectron spectroscopy (UPS) diagram with and without Py-X passivation treatment: UPS spectrum at the beginning of the secondary electron cutoff region (c); the maximum valence band of the Femi level (d); energy level diagrams of $MAPbI_3$ with and without Py-NH_2 passivation treatment (e); energy level alignment of the pristine and Py-NH_2-treated $MAPbI_3$ with the carbon electrode (f).

are corroborated by the observation of the shift of the Pb $4f_{7/2}$ and Pb $4f_{5/2}$ peaks in XPS and of the stretching vibration of the C═N bond in FTIR.

Having determined the influence of Py and Py-NH_2 on the Pb−I bond (the detail is discussed in the Supporting Information), we subsequently investigated their influence on the formation of I vacancies. Figure S11c (PbI_2-terminated surface) and S11d (MAI-terminated surface) demonstrates the defect formation energies (E_{def}) of all the possible I vacancies after the adsorption of Py and Py-NH_2, compared to the clean surface as reference. The overview shows while all I vacancy defects become more difficult to create after the adsorption of Py (the increase in formation energies falls in the range 0.07−0.70 eV) or Py-NH_2 (from 0.15 to 0.86 eV), the most suppressed ones are those directly beneath the Pb atoms on the PbI_2-terminated surfaces. The increase in the formation energy of these vacancies is as large as 0.70 and 0.86 eV for Py and Py-NH_2, respectively, as highlighted in Figure 3d. The increase in the defect formation energies can be explained by the increase in the net atomic charge of Pb after the adsorption of the molecules in Figure 3c, which results in stronger electrostatic interactions of the Pb with the surrounding I species. The most evident increase in the formation energy of the I vacancy beneath the Pb atom can be explained by the increase of net atomic charge of that I atom (from −0.44 to −0.50) as well the Pb atoms (from 0.76 to 0.80) shown in Figure S11a and b.

In brief, combined with experiments, our DFT calculations prove the strong interaction between Py/Py-NH_2 and the $MAPbI_3$ surface, in particular with dangling Pb species. With the treatment of Py/Py-NH_2 on the $MAPbI_3$ surface, effective passivation can be achieved by removing the Pb dangling bonds and increasing the Pb−I bond strength. Both effects help to suppress the migration and the formation of I vacancies and ultimately enhance the structural stability of the perovskites and the operational stability of the devices. We note that although both molecules bind strongly with the perovskite surface, Py-NH_2 exhibits better passivation effect than Py because of more possible binding configurations as well as a more pronounced effect for suppressing the creation of I vacancies.

Steady state photoluminescence (PL) and time-resolved photoluminescence (TRPL) were measured to study the carrier transport properties of passivated perovskite films as shown in Figure 4. All passivated perovskite films deposited on insulating glass substrates showed enhanced PL emission intensity compared with the pristine perovskite film. The Py-NH_2-treated perovskite film presented the strongest PL intensity among all

https://doi.org/10.1021/acsmaterialslett.2c00123
ACS Materials Lett. 2022, 4, 1101−1111

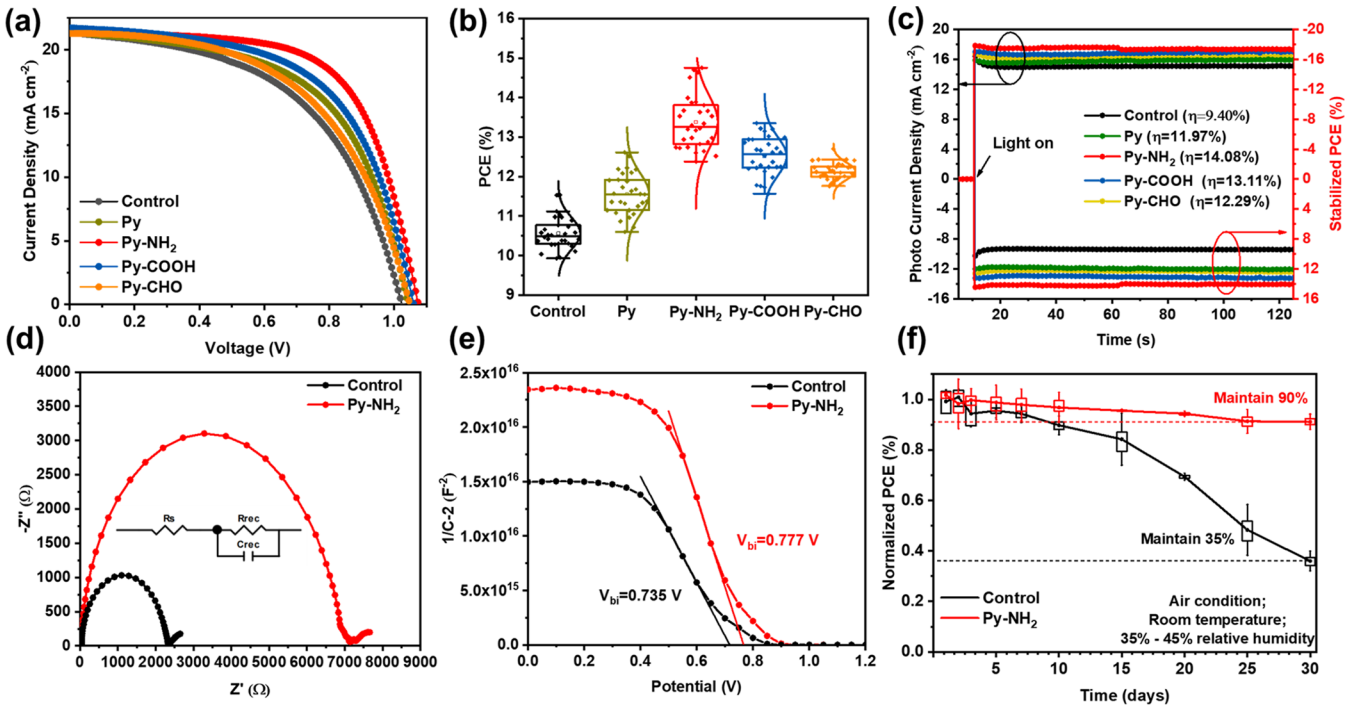

Figure 5. *J*−*V* characteristic curves of perovskite solar cells passivated with and without different Py-X (a); PCE distribution box diagram (b); Steady state output current and steady state output power at the maximum power point (c); Nyquist plots of PSCs under dark conditions at 0.9 V bias (d); Mott−Schottky (e); PCE change curve of unpackaged devices within 30 days (f), Store in air with a relative humidity of 35%−45% at room temperature.

the films, indicating that the film quality was enhanced, the defect state was reduced, and the carrier recombination of the film was effectively minimized.[30,31] Moreover, the PL emission peak center of the Py-NH_2-treated perovskite films shows a blue shift, and it indicates that surface defects are passivated and reduced the trap density near the region of perovskite's band edge.[32] Figure S13a and c (Supporting Information) shows the UV−visible absorption of these films and the PL emission spectra of the films covered by a carbon electrode, respectively. The absorption intensities of the original and passivated perovskite films show similar properties in the wavelength range 500−850 nm. The PL intensity decreases significantly after Py-X surface passivation, proving that carrier transport at the interface of perovskite and the carbon electrode is more efficient after passivation.[12]

The time-resolved PL spectra of perovskite films in Figure 4b show double exponential decay, which can be divided into fast and slow decay processes. The fast decay is attributed to the nonradiative recombination process induced by charge trapping, while the slow decay is related to the carrier recombination process.[19,33,34] The fitting parameters are listed in Table S5. The TRPL attenuation curve is fitted by the double exponential attenuation function[35,36] $f(t) = A_1 \exp\left(\frac{t}{\tau_1}\right) + A_2 \exp\left(\frac{t}{\tau_2}\right)$, where A_1 and A_2 are the relative amplitudes and τ_1 and τ_2 are the carrier lifetimes of fast recombination and slow recombination, respectively. The average carrier lifetime is estimated by the following formula: $\tau_{avg} = \frac{A_1\tau_1^2 + A_2\tau_2^2}{A_1\tau_1 + A_2\tau_2}$. Compared with the original perovskite film (τ_{avg} = 16.27 ns), the Py-NH_2 modified perovskite film showed the longest average carrier lifetime of 34.40 ns. In addition, the average carrier lifetime of films treated by the other passivation agents was also increased, i.e. Py, τ_{avg} = 23.62 ns; Py-COOH, τ_{avg} = 31.40 ns; Py-CHO, τ_{avg} = 27.59 ns. These results show that Py-NH_2 surface passivation can obviously reduce the surface defects of perovskite films and inhibit nonradiative recombination.[37] In addition, in order to study the effect of Py-X passivation treatment on carrier transport at the interface between the perovskite film and the carbon electrode, TRPL spectra were measured on a glass/perovskite/carbon film as shown in Supporting Information Figure S13d. The average carrier lifetime τ_{avg} of the Py-NH_2-treated perovskite film showed a value of 24.43 ns, much lower than that of the original perovskite film of 34.38 ns. This suggests that carrier transport at the perovskite/carbon electrode interface is faster and the density of defect states is reduced after surface passivation.

Ultraviolet photoelectron spectroscopy (UPS) of the original and passivated perovskite films was studied to obtain the electronic properties of perovskite films and energy level alignment information. Figure 4c shows UPS spectra of the secondary electron cutoff initiation region of perovskite films before and after passivation. The calculation formula of the Fermi level is $E_F = -(21.22 - E_{cutoff})$ (where E_F is the Fermi level and E_{cutoff} is the high binding energy cutoff). The Fermi level E_F of the original perovskite is −4.672 eV (E_{cutoff} = 16.548 eV), and the maximum value of the valence band (VBM) can be calculated from the Fermi level minus the low binding energy (VBM = $E_F - E_b$ = −5.915 eV). Tauc plots of the original and passivated perovskite films in Figure S14 show the band gap of these perovskite films is about 1.60 eV. After Py-X passivation treatment, the Fermi level and VBM level were significantly increased as shown in Figure 4e, in which E_F = −4.641 eV and VBM = −5.884 eV for the Py modification; E_F = −4.303 eV and VBM = −5.585 eV for the Py-NH_2 modification; E_F = −4.338 eV and VBM= −5.604 eV for the Py-COOH modification; E_F =

https://doi.org/10.1021/acsmaterialslett.2c00123
ACS Materials Lett. 2022, 4, 1101−1111

−4.516 eV and VBM= −5.740 eV for the Py-CHO modification. As shown in Figure 4f, it can be found that the energy offset ($\Delta\mu$) between the VBM of Py-NH_2-treated perovskite $MAPbI_3$ and the work function (WF) of the carbon electrode decreased from 1.051 to 0.721 eV. The upward shift of the VBM is also confirmed by DFT calculation, and it is attributed to formation of a dipole layer induced by the adsorbed molecules at the interface of $MAPbI_3$ and pyridine-based passivation agents shown in Figure S12 (Py-NH_2@$MAPbI_3$ is discussed in the Supporting Information as the example). It further confirms the interaction between Py-NH_2 and the perovskite film. The electronic state of the perovskite surface was changed after surface passivation, resulting in more upward band bending ($\Delta\Phi$ = 0.561 eV) and in it being more conducive for hole extraction than that of the original perovskite films ($\Delta\Phi$ = 0.192 eV). A Schottky barrier may be formed at the interface of $MAPbI_3$/carbon electrode.[38,39] The higher $\Delta\Phi$ value not only prevents reverse transfer of electrons from $MAPbI_3$ to the carbon electrode but also accelerates hole extraction at the $MAPbI_3$/carbon electrode interface.[24] Therefore, good energy level alignment between the Py-NH_2-treated perovskite/carbon inhibits charge recombination and improves the photovoltaic performance of the final device.

To study the surface passivation effect on the photovoltaic performance of carbon-based perovskite solar cells (PSCs), hole-transporting layer (HTM) free PSCs with the structure FTO/c-TiO_2/m-TiO_2/$MAPbI_3$/carbon were fabricated as shown in Figure S15a. From cross-sectional SEM images of the surface passivated perovskite film (Figure S15b), it can be observed that FTO glass was covered by around 320 nm of a TiO_2 electron transport layer, about 640 nm of a $CH_3NH_3PbI_3$ light absorbing layer, and a few nanometers of a thin layer of passivation molecules.

As shown in Figure 5a and the key photovoltaic parameters summarized in Table 1, the champion carbon-based perovskite solar cells (C-PSCs) passivated by reagents of Py, Py-NH_2, Py-COOH, and Py-CHO gained power conversion efficiencies (PCEs) of 12.61%, 14.75%, 13.55%, and 12.70%, respectively. The control C-PSCs had the champion PCE of 11.55% and an average PCE of 10.56%. The device optimization process of passivation agents at different concentrations is provided in Supporting Information Figures S16 and S17. Among all the passivation agents, Py-NH_2-treated C-PSCs showed the best passivation effect to improve solar cell performance. The corresponding photovoltaic parameters of Py-NH_2-treated C-PSCs have the open circuit voltage (V_{oc}) of 1.074 V, the short circuit current (J_{sc}) of 21.461 mA/cm^2, and the fill factor (FF) of 63.95%. The V_{oc} and J_{sc} showed only a slight improvement compared with the other Py-X passivated solar cells. External quantum efficiency (EQE) spectrum of these PSCs are shown in Supporting Information Figure S18. Prominent enhancement for the Py-NH_2 type C-PSCs can be attributed to the higher FF after surface passivation. This might be attributed to effective carrier extraction and passivation of defects.[40] Figure 5b is a box plot of the PCE distribution of C-PSCs; 30 individual cells were fabricated for comparison. The steady-state output of photocurrent and power plots in Figure 5c show that the device passivated by Py-NH_2 has 14.06% steady-state power output, and this is much higher than that of the control cells of 9.42%.

Table 1. Photovoltaic Parameters of Devices with and without Py-X Passivation Treatment

Device	V_{oc}(V)	J_{sc}(mA cm^{-2})	FF (%)	Best PCE (%)	Average PCE (%)
Control	1.025	21.327	52.87	11.55	10.56
Py	1.045	21.349	56.55	12.61	11.56
Py-NH_2	1.074	21.461	63.95	14.75	13.38
Py-COOH	1.062	21.677	58.00	13.35	12.51
Py-CHO	1.050	21.243	56.89	12.70	12.14

To further understand the passivation effects of Py-X on perovskite films, electrochemical impedance spectroscopy (EIS) was carried out to study the charge transfer process at 0.9 V bias under dark conditions. As shown in the Nyquist diagram of Figure 5d, the Py-NH_2-treated PSCs showed a big semicircle with much larger diameter than that of the control PSCs. The inserted circuit is composed of a series resistance (R_s) and a charge recombination resistance (R_{rec}). R_S values are similar for these solar cells, since the cell structures are almost the same. R_{rec} is related to the charge recombination process in the perovskite film.[41] The R_{rec} value for the Py-NH_2-treated PSCs increased to 7282 Ω compared with that of 2429 Ω for the control PSCs. This suggests that charge recombination in the perovskite layer could be effectively inhibited by the Py-NH_2 passivation molecule. The Nyquist plots of PSCs passivated by the other Py-X are shown in Figure S19a, and the parameters are summarized in Table S6.

From Mott−Schottky analysis of the capacitance voltage ($C-V$) curve in Figure 5e and Figure S19b, the built-in potential (V_{bi}) of PSCs is calculated using the following equation:[42]

$$1/C^2 = \frac{2(V_{bi} - V)}{\varepsilon_0 \varepsilon q A^2 N_A}$$

in which ε_0, ε, q, A, and N_A are the vacuum permittivity, relative permittivity of perovskite, basic charge, device area, and carrier concentration, respectively. Py-NH_2 treatment increases the V_{bi} of PSCs from 0.735 to 0.777 V, which is consistent with the increased V_{oc} value in the cells.[43] The relatively higher V_{bi} indicates an improved driving force to separate charge and an extended depletion region for suppressing carrier recombination.[44] Thus, charge accumulation on the Py-NH_2-treated perovskite/carbon electronic interface is reduced and the device performance is improved.[11,45] The higher V_{bi} might be due to the decrease of energy level mismatch as indicated by the UPS result.

The effect of Py-X passivation treatment on device environmental stability is studied by monitoring PCE changes of unencapsulated solar cells stored in air with humidity of 35%−45% at room temperature. Figure 5f shows that the PCE of the Py-NH_2-treated solar cells can maintain 90% of the original PCE after 30 days' storage, while the control PSCs only maintained 35% of the initial PCE for the same period. Figure S20 presents that PSCs passivated by Py, Py-COOH, and Py-CHO retain 73%, 87%, and 70% of the initial PCE, respectively. The water contact angle of the passivated perovskite films in Figure S21 presented that the Py-NH_2-treated perovskite film has the highest contact angle up to 87°, demonstrating that the Py-NH_2 passivation agent can dramatically increase the hydrophobic nature of the perovskite film. This result showed that the Py-NH_2 passivation effectively enhances the long-term stability of the PSCs, contributing to the reduced defect density of the Py-NH_2-treated perovskite surface, enhanced hydrophobic surface, and better interfacial property of the perovskite/carbon.

https://doi.org/10.1021/acsmaterialslett.2c00123
ACS Materials Lett. 2022, 4, 1101−1111

In summary, pyridine and pyridine derivatives Py-X with different functional groups of -NH_2, -COOH, and -CHO were applied to passivate perovskite $CH_3NH_3PbI_3$ films, respectively. Py-NH_2 agent was found to show the best passivation effect to improve the photovoltaic performance of carbon-based perovskite solar cells among all the examined agents because of its synergy passivation effect of two N atoms from the amino group and pyridine ring. The N atoms bind strongly with the uncoordinated Pb^{2+} of perovskite films and reduce I vacancy defects, thus enhancing carrier transport properties as confirmed from steady state and time-resolved photoluminescence measurements. Meanwhile, interactions of different pyridine derivatives Py-X with the corresponding PbI_2 and perovskite films were carefully investigated by XPS, FTIR, and ^{1}H NMR studies, respectively. DFT calculation was adopted to study the interaction of Py/Py-NH_2 and $CH_3NH_3PbI_3$, elucidating the atomic level mechanism of the improved structural stability and reduced defect density due to the Pb−I bond enhancement after the adsorption and passivation of pyridine and its derivatives. The PCE of devices treated by Py-NH_2 showed the highest PCE of 14.75% among the other passivation agents with the reference of only 11.55% PCE for the control PSC. Moreover, the PSCs with Py-NH_2 surface passivation showed significant improvement in long-term stability, maintaining 90% of the initial PCE after 30 days of storage in air with 35−45% relative humidity. Our work provides a rational design guide for purposely choosing multifunctional passivation agents, especially pyridine-based surface passivation agents, to enhance photovoltaic performance and long-term stability.

EXPERIMENT SECTION

Experimental details are provided in Supporting Information.

ASSOCIATED CONTENT

Supporting Information

The Supporting Information is available free of charge at https://pubs.acs.org/doi/10.1021/acsmaterialslett.2c00123.

Experiment section; photographs of original Py-X in DMF solution and the PbI_2-$(Py\text{-}X)_x$ complex; XRD pattern of PbI_2-$(Py\text{-}X)_x$; statistics of film grain size after treatment with different Py-X passivation agents; XRD and SEM of the original perovskite film and perovskite film treated with chlorobenzene (CB); SEM of perovskite films passivated with high concentration passivation agents; atomic force microscopy images, X-ray photoelectron spectroscopy (XPS), and FTIR spectra of perovskite films; proton nuclear magnetic resonance (^{1}H NMR) spectra of Py-X and its mixed solution with PbI_2; details of DFT calculation; adsorption energy of Py-NH_2/Py on different configurations; UV−vis absorption spectra, PL spectra, and TRPL spectra; cross-section SEM of perovskite film; J−V characteristic curves of solar cells treated by the optimized concentration of passivation agents; incident photon-to-electron conversion efficiency (IPCE) curves; Nyquist plots and Mott−Schottky curve of PSCs; PCE change curves of unpackaged cells stored for 30 days; water contact angles measurements; parameters fitted from a Mott−Schottky test and electrochemical impedance test; parameters fitted from TRPL spectra (PDF)

AUTHOR INFORMATION

Corresponding Authors

Tingting Xu − *School of Chemistry and Chemical Engineering, Northwestern Polytechnical University, Xi'an, Shaanxi 710129, China; Frontiers Science Center for Flexible Electronics (FSCFE), Shaanxi Institute of Flexible Electronics (SIFE) & Shaanxi Institute of Biomedical Materials and Engineering (SIBME), Northwestern Polytechnical University (NPU), Xi'an, Shaanxi 710072, China;* orcid.org/0000-0003-0896-3701; Email: tingtingxu@nwpu.edu.cn

Shuxia Tao − *Center for Computational Energy Research, Applied Physics, Eindhoven University of Technology, 5600 MB Eindhoven, The Netherlands; Materials Simulation and Modelling, Department of Applied Physics, Eindhoven University of Technology, 5600 MB Eindhoven, The Netherlands;* orcid.org/0000-0002-3658-8497; Email: S.X.Tao@Tue.nl

Authors

Kai Zou − *School of Chemistry and Chemical Engineering, Northwestern Polytechnical University, Xi'an, Shaanxi 710129, China*

Qihua Li − *Center for Computational Energy Research, Applied Physics, Eindhoven University of Technology, 5600 MB Eindhoven, The Netherlands; Materials Simulation and Modelling, Department of Applied Physics, Eindhoven University of Technology, 5600 MB Eindhoven, The Netherlands*

Jingquan Fan − *School of Chemistry and Chemical Engineering, Northwestern Polytechnical University, Xi'an, Shaanxi 710129, China*

Hebing Tang − *School of Chemistry and Chemical Engineering, Northwestern Polytechnical University, Xi'an, Shaanxi 710129, China*

Lixin Chen − *School of Chemistry and Chemical Engineering, Northwestern Polytechnical University, Xi'an, Shaanxi 710129, China;* orcid.org/0000-0002-5992-481X

Wei Huang − *Frontiers Science Center for Flexible Electronics (FSCFE), Shaanxi Institute of Flexible Electronics (SIFE) & Shaanxi Institute of Biomedical Materials and Engineering (SIBME), Northwestern Polytechnical University (NPU), Xi'an, Shaanxi 710072, China*

Complete contact information is available at: https://pubs.acs.org/10.1021/acsmaterialslett.2c00123

Author Contributions

†K. Z. and Q. L. contributed equally to this work.

Notes

The authors declare no competing financial interest.

ACKNOWLEDGMENTS

The authors sincerely acknowledge the financial support from the National Key R&D Program of China (2019YFB1503200), the National Natural Science Foundation of China (51972274), China Postdoctoral Science Foundation (2019M653730), and the Open Grants from Analytical & Testing Center of Northwestern Polytechnical University (2020T013). S. T. acknowledges funding from the Computational Sciences for Energy Research tenure track programme of Shell, NWO, and FOM (project no. 15CST04-2) and NWO START-UP, The Netherlands. Q. L. is thankful for the "China Scholarship Council" fellowship (CSC).

REFERENCES

(1) Dong, Q.; Fang, Y.; Shao, Y.; Mulligan, P.; Qiu, J.; Cao, L.; Huang, J. Electron-hole Diffusion Lengths > 175 μm in Solution-grown $CH_3NH_3PbI_3$ Single Crystals. *Science* **2015**, *347*, 967−970.

(2) Jinhui, T.; Zhaoning, S.; Dong Hoe, K.; Xihan, C.; Cong, C.; Kai, Z. Carrier lifetimes of > 1 μs in Sn-Pb Perovskites Enable Efficient All-perovskite Tandem Solar Cells. *Science* **2019**, *364*, 475−479.

(3) Kojima, A.; Teshima, K.; Shirai, Y.; Miyasaka, T. Organometal Halide Perovskites as Visible-light Sensitizers for Photovoltaic Cells. *J. Am. Chem. Soc.* **2009**, *131*, 6050−6051.

(4) Kim, M.; Jeong, J.; Lu, H.; Lee, T. K.; Eickemeyer, F. T.; Liu, Y.; Choi, I. W.; Choi, S. J.; Jo, Y.; Kim, H.-B.; et al. Conformal Quantum Dot-SnO_2 Layers as Electron Transporters for Efficient Perovskite Solar Cells. *Science* **2022**, *375*, 302−306.

(5) Noel, N. K.; Habisreutinger, S. N.; Pellaroque, A.; Pulvirenti, F.; Wenger, B.; Zhang, F.; Lin, Y.-H.; Reid, O. G.; Leisen, J.; Zhang, Y. Interfacial Charge-transfer Doping of Metal Halide Perovskites for High Performance Photovoltaics. *Energy Environ. Sci.* **2019**, *12*, 3063−3073.

(6) Xu, T.; Kong, D.; Tang, H.; Qin, X.; Li, X.; Gurung, A.; Kou, K.; Chen, L.; Qiao, Q.; Huang, W. Transparent MoS_2/PEDOT Composite Counter Electrodes for Bifacial Dye-Sensitized Solar Cells. *ACS Omega* **2020**, *5*, 8687−8696.

(7) Sherkar, T. S.; Momblona, C.; Gil-Escrig, L.; Ávila, J.; Sessolo, M.; Bolink, H. J.; Koster, L. J. A. Recombination in Perovskite Solar Cells: Significance of Grain Boundaries, Interface Traps, and Defect Ions. *ACS Energy Lett.* **2017**, *2*, 1214−1222.

(8) Gao, F.; Zhao, Y.; Zhang, X.; You, J. Recent Progresses on Defect Passivation toward Efficient Perovskite Solar Cells. *Adv. Energy Mater.* **2020**, *10*, 1902650.

(9) Juarez-Perez, E. J.; Hawash, Z.; Raga, S. R.; Ono, L. K.; Qi, Y. Thermal Degradation of $CH_3NH_3PbI_3$ Perovskite into NH_3 and CH_3I Gases Observed by Coupled Thermogravimetry−mass pectrometry Analysis. *Energy Environ. Sci.* **2016**, *9*, 3406−3410.

(10) Noel, N. K.; Abate, A.; Stranks, S. D.; Parrott, E. S.; Burlakov, V. M.; Goriely, A.; Snaith, H. J. Enhanced Photoluminescence and Solar Cell Performance via Lewis Base Passivation of Organic−Inorganic Lead Halide Perovskites. *ACS Nano* **2014**, *8*, 9815−9821.

(11) Han, Y.; Zhao, H.; Duan, C.; Yang, S.; Yang, Z.; Liu, Z.; Liu, S. Controlled N-Doping in Air-Stable $CsPbI_2Br$ Perovskite Solar Cells with a Record Efficiency of 16.79%. *Adv. Funct. Mater.* **2020**, *30*, 1909972.

(12) Hou, M.; Xu, Y.; Zhou, B.; Tian, Y.; Wu, Y.; Zhang, D.; Wang, G.; Li, B.; Ren, H.; Li, Y.; et al. Aryl Diammonium Iodide Passivation for Efficient and Stable Hybrid Organ-Inorganic Perovskite Solar Cells. *Adv. Funct. Mater.* **2020**, *30*, 2002366.

(13) Yang, Z.; Dou, J.; Kou, S.; Dang, J.; Ji, Y.; Yang, G.; Wu, W. Q.; Kuang, D. B.; Wang, M. Multifunctional Phosphorus-Containing Lewis Acid and Base Passivation Enabling Efficient and Moisture-Stable Perovskite Solar Cells. *Adv. Funct. Mater.* **2020**, *30*, 1910710.

(14) Liu, B.; Bi, H.; He, D.; Bai, L.; Wang, W.; Yuan, H.; Song, Q.; Su, P.; Zang, Z.; Zhou, T.; et al. Interfacial Defect Passivation and Stress Release via Multi-Active-Site Ligand Anchoring Enables Efficient and Stable Methylammonium-Free Perovskite Solar Cells. *ACS Energy Lett.* **2021**, *6*, 2526−2538.

(15) Lee, S.-H.; Jeong, S.; Seo, S.; Shin, H.; Ma, C.; Park, N.-G. Acid Dissociation Constant: A Criterion for Selecting Passivation Agents in Perovskite Solar Cells. *ACS Energy Lett.* **2021**, *6*, 1612−1621.

(16) Yang, S.; Dai, J.; Yu, Z.; Shao, Y.; Zhou, Y.; Xiao, X.; Zeng, X. C.; Huang, J. Tailoring Passivation Molecular Structures for Extremely Small Open-Circuit Voltage Loss in Perovskite Solar Cells. *J. Am. Chem. Soc.* **2019**, *141*, 5781−5787.

(17) Wang, R.; Xue, J.; Meng, L.; Lee, J.-W.; Zhao, Z.; Sun, P.; Cai, L.; Huang, T.; Wang, Z.; Wang, Z.-K.; et al. Caffeine Improves the Performance and Thermal Stability of Perovskite Solar Cells. *Joule* **2019**, *3*, 1464−1477.

(18) Peng, J.; Khan, J. I.; Liu, W.; Ugur, E.; Duong, T.; Wu, Y.; Shen, H.; Wang, K.; Dang, H.; Aydin, E.; et al. A Universal Double-Side Passivation for High Open-Circuit Voltage in Perovskite Solar Cells: Role of Carbonyl Groups in Poly(methyl methacrylate). *Adv. Energy Mater.* **2018**, *8*, 1801208.

(19) Qi, C.; Yongjiang, L.; Hong, Z.; Jiabao, Y.; Jian, H.; Xuanhua, L.; Michael, G. Efficient and Stable Inverted Perovskite Solar Cells with Very High Fill Factors via Incorporation of Star-shaped Polymer. *Sci. Adv.* **2021**, *7*, eabg0633.

(20) Laskar, M. A. R.; Luo, W.; Ghimire, N.; Chowdhury, A. H.; Bahrami, B.; Gurung, A.; Reza, K. M.; Pathak, R.; Bobba, R. S.; Lamsal, B. S.; et al. Phenylhydrazinium Iodide for Surface Passivation and Defects Suppression in Perovskite Solar Cell. *Adv. Funct. Mater.* **2020**, *30*, 2000778.

(21) Zou, Y.; Liang, Y.; Mu, C.; Zhang, J. P. Enhancement of Open-Circuit Voltage of Perovskite Solar Cells by Interfacial Modification with p-Aminobenzoic Acid. *Adv. Mater. Interfaces* **2020**, *7*, 1901584.

(22) Zhang, H.; Wu, Y.; Shen, C.; Li, E.; Yan, C.; Zhang, W.; Tian, H.; Han, L.; Zhu, W. H. Efficient and Stable Chemical Passivation on Perovskite Surface via Bidentate Anchoring. *Adv. Energy Mater.* **2019**, *9*, 1803573.

(23) Zhao, Y.; Zhu, P.; Huang, S.; Tan, S.; Wang, M.; Wang, R.; Xue, J.; Han, T. H.; Lee, S. J.; Zhang, A.; et al. Molecular Interaction Regulates the Performance and Longevity of Defect Passivation for Metal Halide Perovskite Solar Cells. *J. Am. Chem. Soc.* **2020**, *142*, 20071−20079.

(24) Wu, Z.; Liu, Z.; Hu, Z.; Hawash, Z.; Qiu, L.; Jiang, Y.; Ono, L. K.; Qi, Y. Highly Efficient and Stable Perovskite Solar Cells via Modification of Energy Levels at the Perovskite/Carbon Electrode Interface. *Adv. Mater.* **2019**, *31*, e1804284.

(25) Tang, H.; Xu, T.; Qin, X.; Zou, K.; Lv, S.; Fan, J.; Huang, T.; Chen, L.; Huang, W. Carbon Quantum Dot-Passivated Perovskite/Carbon Electrodes for Stable Solar Cells. *ACS Appl. Nano Mater.* **2021**, *4*, 13339−13351.

(26) Xu, T.; Zou, K.; Lv, S.; Tang, H.; Zhang, Y.; Chen, Y.; Chen, L.; Li, Z.; Huang, W. Efficient and Stable Carbon-Based Perovskite Solar Cells via Passivation by a Multifunctional Hydrophobic Molecule with Bidentate Anchors. *ACS Appl. Mater. Interfaces* **2021**, *13*, 16485−16497.

(27) Liu, W.; Liu, N.; Ji, S.; Hua, H.; Ma, Y.; Hu, R.; Zhang, J.; Chu, L.; Li, X.; Huang, W. Perfection of Perovskite Grain Boundary Passivation by Rhodium Incorporation for Efficient and Stable Solar Cells. *Nano-Micro Lett.* **2020**, *12*, 119.

(28) Cai, Y.; Cui, J.; Chen, M.; Zhang, M.; Han, Y.; Qian, F.; Zhao, H.; Yang, S.; Yang, Z.; Bian, H.; et al. Multifunctional Enhancement for Highly Stable and Efficient Perovskite Solar Cells. *Adv. Funct. Mater.* **2021**, *31*, 2005776.

(29) Zhuang, J.; Mao, P.; Luan, Y.; Yi, X.; Tu, Z.; Zhang, Y.; Yi, Y.; Wei, Y.; Chen, N.; Lin, T.; et al. Interfacial Passivation for Perovskite Solar Cells: The Effects of the Functional Group in Phenethylammonium Iodide. *ACS Energy Lett.* **2019**, *4*, 2913−2921.

(30) Kanda, H.; Shibayama, N.; Huckaba, A. J.; Lee, Y.; Paek, S.; Klipfel, N.; Roldán-Carmona, C.; Queloz, V. I. E.; Grancini, G.; Zhang, Y.; et al. Band-bending Induced Passivation: High Performance and Stable Perovskite Solar Cells Using a Perhydropoly(silazane) Precursor. *Energy Environ. Sci.* **2020**, *13*, 1222−1230.

(31) Wu, J.; Zhang, W.; Wang, Q.; Liu, S.; Du, J.; Mei, A.; Rong, Y.; Hu, Y.; Han, H. A Favored Crystal Orientation for Efficient Printable Mesoscopic Perovskite Solar Cells. *J. Mater. Chem. A* **2020**, *8*, 11148−11154.

(32) Wu, X.; Zhang, L.; Xu, Z.; Olthof, S.; Ren, X.; Liu, Y.; Yang, D.; Gao, F.; Liu, S. Efficient Perovskite Solar Cells via Surface Passivation by a Multifunctional Small Organic Ionic Compound. *J. Mater. Chem. A* **2020**, *8*, 8313−8322.

(33) Su, T. S.; Eickemeyer, F. T.; Hope, M. A.; Jahanbakhshi, F.; Mladenovic, M.; Li, J.; Zhou, Z.; Mishra, A.; Yum, J. H.; Ren, D.; et al. Crown Ether Modulation Enables over 23% Efficient Formamidinium-Based Perovskite Solar Cells. *J. Am. Chem. Soc.* **2020**, *142*, 19980−19991.

(34) Xu, T.; Wan, Z.; Tang, H.; Zhao, C.; Lv, S.; Chen, Y.; Chen, L.; Qiao, Q.; Huang, W. Carbon Quantum Dot Additive Engineering for

https://doi.org/10.1021/acsmaterialslett.2c00123
ACS Materials Lett. 2022, 4, 1101−1111

Efficient and Stable Carbon-Based Perovskite Solar Cells. *J. Alloys Compd.* **2021**, *859*, 157784.
(35) Hanmandlu, C.; Swamy, S.; Singh, A.; Hsin-An, C.; Liu, C.-C.; Lai, C.-S.; Mohapatra, A.; Pao, C.-W.; Chen, P.; Chu, C.-W. Suppression of Surface Defects to Achieve Hysteresis-free Inverted Perovskite Solar Cells via Quantum Dot Passivation. *J. Mater. Chem. A* **2020**, *8*, 5263−5274.
(36) Cai, Y.; Cui, J.; Chen, M.; Zhang, M.; Han, Y.; Qian, F.; Zhao, H.; Yang, S.; Yang, Z.; Bian, H.; et al. Multifunctional Enhancement for Highly Stable and Efficient Perovskite Solar Cells. *Adv. Funct. Mater.* **2021**, *31*, 2005776.
(37) Yuan, S.; Qian, F.; Yang, S.; Cai, Y.; Wang, Q.; Sun, J.; Liu, Z.; Liu, S. NbF5: A Novel α-Phase Stabilizer for FA-Based Perovskite Solar Cells with High Efficiency. *Adv. Funct. Mater.* **2019**, *29*, 1807850.
(38) Wu, W. Q.; Wang, Q.; Fang, Y.; Shao, Y.; Tang, S.; Deng, Y.; Lu, H.; Liu, Y.; Li, T.; Yang, Z.; et al. Molecular Doping Enabled Scalable Blading of Efficient Hole-Transport-Layer-Free Perovskite Solar Cells. *Nat. Commun.* **2018**, *9*, 1625.
(39) Zhang, G.; Xie, P.; Huang, Z.; Yang, Z.; Pan, Z.; Fang, Y.; Rao, H.; Zhong, X. Modification of Energy Level Alignment for Boosting Carbon-Based $CsPbI_2Br$ Solar Cells with 14% Certified Efficiency. *Adv. Funct. Mater.* **2021**, *31*, 2011187.
(40) Ma, Z.; Zhou, W.; Huang, D.; Liu, Q.; Xiao, Z.; Jiang, H.; Yang, Z.; Zhang, W.; Huang, Y. Nicotinamide as Additive for Microcrystalline and Defect Passivated Perovskite Solar Cells with 21.7% Efficiency. *ACS Appl. Mater. Interfaces* **2020**, *12*, 52500−52508.
(41) Li, T.; Wang, S.; Yang, J.; Pu, X.; Gao, B.; He, Z.; Cao, Q.; Han, J.; Li, X. Multiple Functional Groups Synergistically Improve the Performance of Inverted Planar Perovskite Solar Cells. *Nano Energy* **2021**, *82*, 105742.
(42) Zhang, Z.; Gao, Y.; Li, Z.; Qiao, L.; Xiong, Q.; Deng, L.; Zhang, Z.; Long, R.; Zhou, Q.; Du, Y. Marked Passivation Effect of Naphthalene-1, 8-Dicarboximides in High-Performance Perovskite Solar Cells. *Adv. Mater.* **2021**, *33*, 2008405.
(43) Jung, E. H.; Jeon, N. J.; Park, E. Y.; Moon, C. S.; Shin, T. J.; Yang, T. Y.; Noh, J. H.; Seo, J. Efficient, Stable and Scalable Perovskite Solar Cells Using Poly(3-hexylthiophene). *Nature* **2019**, *567*, 511−515.
(44) Li, G.; Song, J.; Wu, J.; Song, Z.; Wang, X.; Sun, W.; Fan, L.; Lin, J.; Huang, M.; Lan, Z.; et al. Efficient and Stable 2D@3D/2D Perovskite Solar Cells Based on Dual Optimization of Grain Boundary and Interface. *ACS Energy Lett.* **2021**, *6*, 3614−3623.
(45) Zhang, J.; Bai, D.; Jin, Z.; Bian, H.; Wang, K.; Sun, J.; Wang, Q.; Liu, S. F. 3D-2D-0D Interface Profiling for Record Efficiency All-Inorganic $CsPbBrI_2$ Perovskite Solar Cells with Superior Stability. *Adv. Energy Mater.* **2018**, *8*, 1703246.

https://doi.org/10.1021/acsmaterialslett.2c00123
ACS Materials Lett. 2022, 4, 1101−1111